A Wavelet Based Suboptimal Kalman Filter for Assimilation of Stratospheric Chemcial Tracer Observations

Ludovic Auger
METEO FRANCE, Toulouse, France

and

Andrew Tangborn*
Data Assimilation Office NASA-GSFC, Greenbelt, MD
and
JCET, University of Maryland-Baltimore County, Baltimore, MD

May 28, 2002

To be submitted to *Monthly Weather Review*

*Corresponding author address: Dr. Andrew Tangborn, Data Assimilation Office, Code 910.3, Goddard Space Flight Center, Greenbelt, MD 20771. E-mail: tangborn@dao.gsfc.nasa.gov

Abstract

A suboptimal Kalman filter system which evolves error covariances in terms of a truncated set of wavelet coefficients has been developed for the assimilation of chemical tracer observations of CH_4. The truncation is carried out in such a way that the resolution of the error covariance is reduced only in the zonal direction, where gradients are smaller. Assimilation experiments which last 24 days, and used different degrees of truncation were carried out. These reduced the covariance by 90, 97 and 99 % and the computational cost of covariance propagation by 80, 93 and 96 % respectively. The difference in both error covariance and the tracer field between the truncated and full systems over this period were found to be not growing in the first case, and growing relatively slowly in the later two cases. The largest errors in the tracer fields were found to occur in regions of largest zonal gradients in the tracer field.

1 Introduction

The development of sub-optimal Kalman filter schemes for data assimilation has been motivated by the need to reduce the computational expense of evolving error covariances. These techniques can be roughly divided into representation by truncated expansion, Monte-Carlo and flow dependent covariance methods. Truncated expansion methods use an efficient representation of the error covariance and its propagator, such as SVD (Tippet *et al.* 2000), (Farrel and Iannou 2001), eigendecomposition (Cohn and Todling, 1996) or wavelets (Chin *et al.*, 1996), (Tangborn and Zhang, 2000). These can then be truncated to a few leading terms leading to a low dimensional system. The Monte-Carlo or ensemble Kalman filter method (Evensen, 1994) (Houtekamer and Mitchell, 1998) avoids the expense of propagating error covariances by estimating them from an ensemble of short range forecasts. This approach also has the advantage of obtaining current ensemble statistics instead of relying on a tangent linear model (TLM) to evolve sometimes questionable initial error statistics. However, computational limitations generally allow for ensemble sizes in the hundreds, and therefore the possibility of spurious solutions require the truncation of covariances for large distances. Flow dependent error covariance (Riishøjgaard, 1998), assumes that the background error correlation has essentially the same shape as the background field. This approach has the potential to estimate anisotropic correlations with only a slightly higher computational cost than isotropic error correlations.

All of these approaches have goal of estimating local, anisotropic error correlations. An important step in determining whether a given method has the potential to be implemented in a realistic large scale assimilation system. A Wavelet basis is a logical means for representing both the error covariances and the TLM, because the approximation is local in position and scale. Not only is this representation highly compressive for anisotropic data, but it gives explicit information on the location and scale of the most important covariance structures. This allows for adaptive schemes to truncate the wavelet expansion to a small number of significant terms, and potentially could provide insight into the relationship between important features in the error covariance and background fields.

Recent work on Kalman filtering of chemical tracer observations (Ménard *et al.*, 2000 and

Ménard and Chang, 2000) has provided a benchmark with which to test suboptimal schemes for tracer assimilation. In this system, chemical species observations (*eg.* CH_4) from limb-sounding instruments (CLAES and HALOE) are assimilated into a global two-dimensional transport model on isentropic surfaces. All of the necessary specifications, including initial, model and observational error covariances, are designed and tested in this work. Testing of a number of simplifying assumptions that eliminate vertical error correlations of observations, diabatic effects, vertical mixing and chemical sources and sinks are also done. The results of this work show the error covariances do have some state dependence. They also discovered that there is signficant loss of error variance due to "spurious dissipation in the small scale covariance structures". This problem was overcome by introducing a variace correction term that keeps the total error variance constant during the forecast propagation step (and before the addition of model error). The complexities of propagating the error covariance in wavelet space make this variance correction step unviable. Therefore the variance loss issue is not considered in the present work.

In this study, we have taken the Kalman filter system developed by Ménard *et al.* and project the error covariances and covariance propagator (transport model) onto an orthonormal wavelet basis. The resulting system then carries out the propagation of error covariances in "wavelet space". Several different levels of truncation are used and all of the results are compared with the *benchmark* code in terms of error covariance, the constituent field and computational time. While the full system does not represent the true state, its behavior is well understood, and we seek to understand how this low dimensional representation effects the covariance evolution, and how this in turn effects the assimilated constituent field.

2 The Transport Advection Scheme and Constituent Assimilation System

The details of the Kalman filter Assimilation scheme are given in Menard *et al.* (2000), and we give a summary here. The evolution of a chemical constituent field along an isentropic surface is governed by

$$\frac{\partial \mu^t}{\partial t} + \mathbf{V} \cdot \nabla \mu^t = f, \tag{1}$$

where μ^t is the true tracer mixing ratio, $\mathbf{V}$ is the horizontal wind field along an isentropic surface and ∇ is the horizontal gradient operator restricted to the isentropic surface. The true state of any constituent field will depend on chemical reaction (source and sink) and diffusion, and are represented by the random forcing term f. The model used to make forecasts is conservative and ignores the sources, sinks and diffusion, so that f is set to zero in the transport code.

The numerical model used to solve the transport equation is adapted from the Lin and Rood (1996) scheme which uses the conservative form

$$\frac{\partial \mu}{\partial t} + \nabla \cdot (\mu \mathbf{V}) = \mu \nabla \cdot \mathbf{V}, \tag{2}$$

and is solved by an operator splitting approach. The system is solved off-line using wind analyses $\mathbf{V}$ produced by the Goddard Earth Observing Data Assimilation System (GEOS-DAS). The discretized equations have the form

$$\mu_{k+1} = \mathbf{M}_k \mu_k \tag{3}$$

where μ_k is the mixing ratio at time t_k and $\mathbf{M}_k$ the discretized transport model from t_k to t_{k+1}. Model error ϵ_k^q in (3) come from discretization and the neglected right hand side of 1. ϵ_k^q is assumed to have zero bias and normally distributed, with associated covariance $\mathbf{Q}_q$. Menard *et al.* (2000) showed that the model error is state dependent, using the form

$$\mathbf{Q}_k(i,j) = \delta^2 \mu_k^a(i) \mu_k^a(j) \mathbf{C}^q(i,j), \tag{4}$$

where the correlation $\mathbf{C}^q(i,j)$ is given by

$$\mathbf{C}^q(i,j) = \exp\left(\frac{-|\mathbf{r}_i - \mathbf{r}_j|}{L}\right). \tag{5}$$

L is the correlation length scale, $\mathbf{r}_i$ and $\mathbf{r}_j$ are position vectors of two points on the sphere, and δ is a relative error parameter. The initial error covariance matrix takes the same form as the model error covariance

$$\mathbf{P}_0(i,j) = \gamma^2 \mu_0(i) \mu_0(j) \mathbf{C}(i,j) \tag{6}$$

where $\mathbf{C}(i,j)$ is the same as in (5).

The observations of mixing ratios at time t_k, μ_k^o, can be related to the true mixing ratio by

$$\mu_k^o = \mathbf{H}_k \mu_k^t + \epsilon_k^o \tag{7}$$

where ϵ_k^o is the observation error, which includes contributions from measurement, retrieval and representativeness errors. The observation error is assumed unbiased, normally distributed and state independent, and has associated covariance matrix $\mathbf{R}_k^o$.

The Kalman filter algorithm consists of the forecast step

$$\mu_{k+1}^f = \mathbf{M}_k \mu_k^a \tag{8}$$

$$\mathbf{P}_{k+1}^f = \mathbf{M}_k \mathbf{P}_k^a \mathbf{M}_k^T + \mathbf{Q}_k \tag{9}$$

and the analysis step

$$\mu_{k+1}^a = \mu_{k+1}^f + \mathbf{K}_{k+1}(\mu_{k+1}^o - \mathbf{H}_{k+1}\mu_{\mathbf{k+1}}^{\mathbf{f}}) \tag{10}$$

$$\mathbf{P}_{k+1}^a = (\mathbf{I} - \mathbf{K}_{k+1}\mathbf{H}_{k+1})[(\mathbf{I} - \mathbf{K}_{k+1}\mathbf{H}_{k+1})\mathbf{P}_{k+1}^f]^T + \mathbf{K}_{k+1}\mathbf{R}_{k+1}^o\mathbf{K}_{k+1}^T \tag{11}$$

where the Kalman gain matrix $\mathbf{K}_k$ is given by

$$\mathbf{K}_{k+1} = (\mathbf{H}_{k+1}\mathbf{P}_{k+1}^f)^T(\mathbf{H}_{k+1}\mathbf{P}_{k+1}^f\mathbf{H}_{k+1}^T + \mathbf{R}_{k+1}^o)^{-1} \tag{12}$$

The error covariance dynamics, (9), are computed by Menard *et al.* using a two-step scheme that corrects for variance loss. The forecast error covariance is initially computed as

$$\mathbf{P}_{k+1}^f = \mathbf{M}_k \mathbf{P}_k^a \mathbf{M}_k \tag{13}$$

and the error variance is treated as a conserved scaler and computed as

$$\mathbf{V}_{k+1}^f = \mathbf{M}_k \mathbf{V}_k^a \tag{14}$$

The computational grid for this assimilation is 72×46.

3 Wavelet Representation of Error Covariances

Wavelets are a family of basis functions with local support. They are generated from scaling functions which satisfy the recursion relationship

$$\phi(x) = \sum_k c_k \phi(2x - k) \tag{15}$$

where the choice of filter coefficients c_k determines the properties of the resulting scaling function and wavelet. A small number of non-zero c_k will give rise to more localized wavelets and a larger number of c_k will produce smoother (*i.e.* continuous higher derivatives) wavelets. The basic Wavelet function, ψ, for a given set of filter coefficients can be derived from scaling functions by taking differences

$$\psi(x) = \sum_k (-1)^k c_{1-k} \phi(2x - k). \tag{16}$$

The representations of different scales and locations are then obtained by dilating and translating $\psi(x)$

$$\psi_{j,k}(x) = 2^{j/2} \psi(2^j x - k) \tag{17}$$

where j refers to dilation (scale) and k refers to translation (location).

Representation of a function in two dimensions is similar to Fourier or other bases, we use the product of two functions:

$$P(x, y) = \hat{P_{j_x,k_x,j_y,k_y}} \psi_{j_x,k_x}(x) \psi_{j_y,k_y}(y) \tag{18}$$

where $\hat{P_{jx,kx,jy,ky}}$ is the wavelet coefficient for scales j_x, j_y and locations k_x, k_y. The scales and translations in each direction are varied independently of each other.

We are employing the discrete wavelet transform, because we wish to represent a covariance matrix by its wavelet coefficients. The pyrimidal wavelet transform of Mallet (1989) recursively determines the coefficients at each scale, from finest to coarsest, by calculating weighted averages and differences at each scale. The transform from the physical space covariance to wavelet representation is then

$$\hat{\mathbf{P}} = \mathbf{W}\mathbf{P}\mathbf{W}^T \tag{19}$$

where $\mathbf{P}$ and $\hat{\mathbf{P}}$ are the physical and wavelet space covariance matrices and $\mathbf{W}$, $\mathbf{W}^T$ represent the wavelet transform and it's transpose. For and $N \times N$ matrix, and the transform requires $o(N^2)$ operations.

In order to understand the structure of the matrix that is to be represented by a wavelet basis, we plot an example of the entire error covariance in Fig. 1. The (x,y) coordinates are collapsed into a single vector (with x incremented in the inner loop). The covariance at a single point makes up a single column in the covariance, as shown in Fig. 2. The

next column in the matrix will be the covariance for the grid point just to the right, and so on. The vertical and horizontal variations in Fig. 1 each represent the covariance of one point over the entire domain. The finest scales represent the smallest scale structures in the x-direction while y-direction variations are at larger scales. Therefore a trunction to L=1024 coefficients will mean that the two finest scales (j=11,12, corresponding to $5 - 10^o$ resolution) are removed in the zonal direction. Because of the structure of the error covariance, no information in the meridional direction is lost by this truncation. Since the steepest gradients in both the constituent field and the error covariance are in the meridional direction, we expect the Kalman filter to be most sensitive to loss of spatial information in this direction.

4 Description of the Assimilation Scheme in Wavelet Space

We consider two schemes for carrying out the propagation of error covariances in wavelet space. In the first, the analysis covariance and the transport model are projected onto a wavelet wavelet basis and the covariance is propagated in wavelet space. The covariance is then transformed back to physical space and the analysis covariance and Kalman gain are calculated. The second approach leaves the analysis covariance in wavelet space and also calculates the Kalman gain in wavelet space. The former ensures that the non-uniform observation locations helps to introduce new wavelet coefficients in adaptive schemes while the latter eliminates the need for forward and backward wavelet transforms at each analysis time.

We use a wavelet transform that comes from the family of compactly supported orthonormal wavelets introduced by Daubechies (1988). The fast discrete transform of Mallat (1989) is employed, and applied to the error covariance,

$$\hat{\mathbf{P}} = \mathbf{W}\mathbf{P}\mathbf{W}^T \tag{20}$$

where $\mathbf{W}$, $\mathbf{W}^T$ represent the wavelet transform and its transpose, and $\hat{\mathbf{P}}$ is the wavelet representation of $\mathbf{P}$. The fast wavelet transform requires a vector length be a power of 2, so we use zero padding to increase the grid to 128×64 , and $\mathbf{P}$ becomes a $N_p \times N_p = 4096 \times 4096$ matrix.

Computation of the model dynamics in wavelet space requires a bit more work because it is an operator rather than a matrix. However, M_k can be computed by applying the model operator to the identity matrix. We then compute the wavelet representation of the model dynamics

$$\hat{\mathrm{M}}_k = \mathbf{W}\mathrm{M}_k\mathbf{W}^T \tag{21}$$

The approximation of the covariance and model dynamics is made through truncation of (20) and (21), in order to make use of the efficient representation of localized structures afforded by the wavelet representation. We consider to approaches to truncation: retention of the largest scales and retention of the scales with the largest variance. Experiments using these approaches will be described in the next section.

(a) Forecast in Wavelet Space/Analysis in Physical Space

Updating of μ^f remains the same,

$$\mu^f_{k+1} = \mathrm{M}_k\mu^a_k \tag{22}$$

while the previous analysis error covariance, model dynamics and model error are projected onto the wavelet basis,

$$\hat{\mathbf{P}}^a = \mathbf{W}\mathbf{P}^a_k\mathbf{W}^T \tag{23}$$

$$\hat{\mathrm{M}}_k = \mathbf{W}\mathrm{M}_k\mathbf{W}^T \tag{24}$$

$$\hat{\mathbf{Q}}_k = \mathbf{W}\mathbf{Q}_k\mathbf{W}^T \tag{25}$$

The covariances and model dynamics are then truncated to L equations, based on either scale or error variance criteria. The truncated covariance is then updated

$$(\hat{\mathbf{P}}^f_{k+1})_L = (\hat{\mathrm{M}}_k)_L(\mathbf{P}^a_k)_L(\hat{\mathrm{M}}^T_k)_L + (\hat{\mathbf{Q}}_k)_L \tag{26}$$

The forecast error covariance is then transformed back to physical space

$$\mathbf{P}^f_{k+1} = \mathbf{W}^T\hat{\mathbf{P}}^f_{k+1}\mathbf{W} \tag{27}$$

and the analysis step

$$\mu^a_{k+1} = \mu^f_{k+1} + \mathbf{K}_{k+1}(\mu^o_{k+1} - \mathbf{H}_{k+1}\mu^{\mathrm{f}}_{\mathbf{k+1}}) \tag{28}$$

$$\mathbf{P}^a_{k+1} = (\mathbf{I} - \mathbf{K}_{k+1}\mathbf{H}_{k+1})[(\mathbf{I} - \mathbf{K}_{k+1}\mathbf{H}_{k+1})\mathbf{P}^f_{k+1}]^T + \mathbf{K}_{k+1}\mathbf{R}^o_{k+1}\mathbf{K}^T_{k+1} \tag{29}$$

where the Kalman gain matrix $\mathbf{K}_k$ is given by

$$\mathbf{K}_{k+1} = (\mathbf{H}_{k+1}\mathbf{P}^f_{k+1})^T(\mathbf{H}_{k+1}\mathbf{P}^f_{k+1}\mathbf{H}^T_{k+1} + \mathbf{R}^o_{k+1})^{-1} \tag{30}$$

(b) Forecast and Analysis Covariance updated in Wavelet Space

This scheme eliminates the need to transform the covariances between physical and wavelet space each analysis time, but what about $\mathbf{Q}_k$ and $\mathbf{M}_k$? $\mathbf{M}_k$ depends on the current winds and is continually changing, so equation (24) is still needed. $\mathbf{Q}_k$ is defined by equation (4) as the product of the original correlation and current variance field. A computationally more efficient scheme for calculating $\hat{\mathbf{Q}}_k$ can be formulated by noting that

$$\mathbf{W}\mathbf{Q}_k\mathbf{W}^T = \delta^2(\mathbf{W}\,[\mu_k]\,\mathbf{W}^T)(\mathbf{W}\mathbf{C}^q\mathbf{W}^T)(\mathbf{W}\,[\mu_k]\,\mathbf{W}^T) \tag{31}$$

where $[\mu_k]$ is a matrix with diagonal elements μ_k. The term $\mathbf{W}\mathbf{C}^q\mathbf{W}^T$ need only be computed once while the first and third terms of (31) must be recomputed each analysis time.

We also note that, since only L rows and columns of each matrix is being retained, the computation of the forward wavelet transforms can be significantly reduced by making use of the structure of the Mallat tree algorithm when the truncation criterion is by scale. The tree algorithm is a series of "averages" and "differences" taken at the finest scales first. This average on each scale is used to calculate the average and difference on the next coarser scale, and the complete set of differences makes up the set of wavelet coefficients. If we are retaining only the L largest coefficients, then only averages need to be taken for the first $N - L$ coefficients. Since $L << N$ for our assimilation, the difference calculation is done for only a small fraction of the matrix.

The assimilation scheme again starts with an update of μ^f

$$\mu^f_{k+1} = \mathbf{M}_k\mu^a_k. \tag{32}$$

Project the model dynamics onto wavelet basis

$$\hat{\mathbf{M}}_k = \mathbf{W}\mathbf{M}_k\mathbf{W}^T \tag{33}$$

Project the mixing ratio contribution onto wavelet basis and compute new model error in wavelet space

$$\hat{\mathbf{Q}}_k = \delta^2(\mathbf{W}[\mu_k]\mathbf{W}^T)\hat{\mathbf{C}}^q(\mathbf{W}[\mu_k]\mathbf{W}^T), \tag{34}$$

where $\hat{\mathbf{C}}^q$ is the initial error correlation model in wavelet space.

Truncate dynamics and model error to L terms and calculate new forecast error covariance in wavelet space:

$$(\hat{\mathbf{P}}^f_{k+1})_L = (\hat{\mathbf{M}}_k)_L(\mathbf{P}^a_k)_L(\hat{\mathbf{M}}^T_k)_L + (\hat{\mathbf{Q}}_k)_L \tag{35}$$

Calculate analysis error covariance in wavelet space

$$\hat{\mathbf{P}}^a_{k+1} = (\mathbf{I} - \hat{\mathbf{K}}_{k+1}\hat{\mathbf{H}}_{k+1})[(\mathbf{I} - \hat{\mathbf{K}}_{k+1}\hat{\mathbf{H}}_{k+1})\hat{\mathbf{P}}^f_{k+1}]^T + \hat{\mathbf{K}}_{k+1}\mathbf{R}^o_{k+1}\hat{\mathbf{K}}^T_k \tag{36}$$

$$\hat{\mathbf{K}}_{k+1} = \mathbf{W}\mathbf{K}_{k+1} \tag{37}$$

$$\hat{\mathbf{H}}_{k+1} = \mathbf{H}_{k+1}\mathbf{W}^T \tag{38}$$

are the Kalman gain and observation operator mixed physical/wavelet space. Notice that $\mathbf{R}^o_{k+1}$ is in physical space, because $\hat{\mathbf{K}}$ and $\hat{\mathbf{K}}^T$ are only right and left multiplied by the wavelet transform matrix respectively.

5 Assimilation Results

Success of any approximate scheme for evolving error covariances is ultimately measured by the accuracy of the analyses themselves and the reduction in computational cost that the scheme achieves. We also wish to understand how well the wavelets represent the covariance and dynamics matrices, and how the accuracy of this representation effects the assimilation accuracy. It is particularly important to understand the relationship between the loss of covariance information and decrease in assimilation accuracy that occurs as the number of coefficients retained is reduced.

In all cases, the computational grid is 46×72, so that each correlation matrix is 46×72 and the full covariance matrix is then $n \times n = 3312 \times 3312$. The fast wavelet transform requires that the system dimension be a power of 2, so we pad the covariance to $n \times n = 4112 \times 4112$. Truncation is carried out on the finest scales first. The finest scale is always

half of the total number of coefficients, removing 2056 wavelet coefficients is equivalent to removing just the $J = 11$ scale, for example.

(a) Forecast Covariance in Wavelet Space

Constituent assimilation using both the full and truncated error covariances have been carried out over a period of 9 days. Truncation to $L = 1024$, resulting in the removal of the two finest ($j = 10, 11$) was used. The correlation for a single point after nine days of assimilation is shown in Fig. 3 for the full system (a), and for $L = 1024$ (b). The correlation that results from the truncated system is seen to be qualitatively and quantitatively very close to the full system correlation. The mean quadratic difference in the constituent fields between the truncated and full systems is shown in Fig. (3)c. The error incurred by truncation of the covariance and the TLM show an initial rapid increase that levels off around 21/2 days. This stabilization indicates that the approximation scheme will not result in long term error growth relative to the full Kalman filter system.

Computational savings for this scheme, however, were found to be rather small. While truncation of the covariance propagation equation reduces the operation count by $(L/N)^2 = (1024/3312)^2 = 1/10$, the scheme requires a forward and back wavelet transform on the entire covariance and a forward transform on the propagator each analysis time. Each transform consists of $o(N_p^2)$, and in this case is carried out twice every 12 timesteps. The computational savings over one analysis cycle due to the wavelet truncation is $o(10^7)$ operations, while the computational cost of the wavelet transforms is also $o(10^7)$. Thus there is no significant savings if the analysis error covariance is calculated in physical space. A further reduction in L will only slightly decrease the computational cost of the propagation step while degrading the accuracy of the error covariance. We conclude that the analysis error covariance needs to be determined in physical space in order to realize any significant computational savings.

(b) Forecast and Analysis Covariance in Wavelet Space

Constituent assimilation was carried out for 24 days (the same initial state as in the previous section) using the approximation scheme in (32-38), with L=1024, 512 and 256. These are again compared with the benchmark assimilation which evolves the full error

covariance in physical space. Error correlations for the node (29,13) are again plotted for each level of approximation and the benchmark in Figure 4 (a). The L=1024 truncation case is seen in panel (b) to accurately reproduce the covariance both in shape and range of values. It is particularly important that the long tail in the covariance field that extends below Africa and over Antarctica is successfully reproduced in the truncated expansion. This feature is less than 5^o in width in the meridional direction, which confirms the fact that the removal of the two finest wavelet scales (j=11,12) only affected zonal direction features to the covariance. Panels (c) and (d) show the covariance for the same location on the 24^{th} day with the covariance evolution system truncated to $L = 512$ and $L = 256$ wavelet coefficients respectively. Both the qualitative shape and range of values of changed significantly here. These more severe truncations remove the (j=9,10) scales from the error covariance, which correspond to resolutions of $20-40^o$ in the zonal direction. It is likely that this level of truncation removes too much of both zonal direction structure and propagator dynamics.

The assimilated constituent field for the benchmark (a) and and the relative error (%)

$$\%error = \frac{\mu_{approx} - \mu_{bench}}{\mu_{bench}} \times 100$$

for three levels of covariance truncation (b-d) are shown in Fig. 5.

As expected the errors increase as L is decreased, but what is interesting is the locations of the maximum errors. For the most part, these maxima occur where there is a steep zonal direction gradient in the constituent field. This can be seen most clearly in panel (c) where the maxima are in the North atlantic and just north of Japan. In both of these locations there are there are dips in the interface between regions of high and low CH_4 concentrations, so that the steepest gradients become locally meridional instead of zonal. This behavior in the difference between the full and approximated Kalman filter can be seen in all levels of truncation and numerous locations. Even though the constituent field is not approximated by truncated wavelet expansions, steep gradients in the concentration field (or fronts) give rise to regions of higher error covariance (and thus gradients in covariance). While these gradients generally run North/South, we have made no approximation to the error covariances in this direction. Thus, whenever the gradient becomes zonal, the loss of resolution in the zonal direction begins to affect the assimilated field.

Not all of the differences in the constituent field can be ascribed to loss of resolution in the zonal direction. Farrel and Iannou (2001) discussed the issue of dynamics truncation, which can lead to errors in covariance propagation at later times because some growing modes may be lost. Also, truncation errors in zonal direction error covariance can lead to more general errors through the propagtor, M.

It is also useful to plot the time evolution of the mean relative error,

$$E_{mean} = \frac{1}{A_{tot}} \sum_{i,j} \frac{|\mu i, j - \mu_{ref}(i,j)|}{\mu_{ref}(i,j)} \Delta A_{i,j}, \tag{39}$$

in the constituent field with respect to the full Kalman filter system, shown in Fig. 6. We define $\Delta A_{i,j}$ as the area increment associated with node (i,j). The mean error in the L=1024 case is seen to stop increasing and actual decrease starting around the 5^{th} day, while the errors L=512,256 cases continue to show a slight tendency to increase even after 24 days. Growing errors are an indication of that propagator truncation is beginning to become a significant source of covariance error.

The reductions in computational costs associated with this scheme over the course of a 24 day assimilation are about 80% for $L = 1024$, 93% for $L = 512$ and 96% for $L = 256$. Each of these are compared with the Kalman filter system with error covariance evolved in physical space. These reductions are roughly 2^{nd} order, inspite of the additional expense of constructing the propagator in matrix from and projecting it onto the wavelet basis each analysis time.

6 Discussion and Conclusions

We have implemented a Kalman filter system for the assimilation of chemical constituent observations from limb-sounding instruments in which the error covariances are propagated forward in terms of their wavelet coefficients. The code has been compared with the benchmark system of Ménard *et al.* (2000) with several different degrees of truncation of the wavelet coefficents. The truncation removes the finest scales first, and only in the zonal direction. Thus, as the number of retained coefficients in the covariance propagation are reduced, increasingly coarser scales are eliminated. The important information that can be obtained from these experiments is the relationship between changes in the error covariances

and the consituent field itself. Since error variances are larger in regions of steep gradients in the constiuent field, the two-point covariances will tend to be alligned in the zonal direction, as is seen in Fig. 4. Structures with this shape will require a lower resolution in the zonal direction, thus allowing the finest scale coefficients in this direction to be eliminated.

These experiments show that as the resolution of the error covariance propagation is reduced, errors in the constituent field will increase first where the gradient of the constituent field is greatest. Within the regions of steep constituent gradients, the largest errors are found to occur where the gradients are steepest in the zonal direction.

While this work does not consider adaptive schemes which vary the local scale retained according to *a priori* estimates of the truncation error, these assimilation results give some insight as to how such a scheme might work. We can take advantage of the fact that steep gradients in the constituent field give rise to larger error variances as well as sharp features in the covariance field. The constituent forecast is updated before the error covariance, so it is available for estimating the location of small scale features in the covariance field. An adaptive scheme of this could be combined with an error covariance estimate from either a flow dependent scheme (Riishojgaard, 1998) or a low order ensemble Kalman filter (*e.g.* Houtekammer and Mitchell, 1998). This would allow the number of wavelet coefficients to be further reduced with a very modest computational expense.

7 References

Cohn, S.E., and R. Todling, Approximate data assimilation schemes for stable and unstable dynamics, *J. Meteol. Soc. of Japan*, **74**, 63-75, 1996.

Daubechies, I., Orthonormal Bases of Compactly Supported Wavelets. *Communications in Pure and Applied Mathematics*, **41**, 909-996, 1998.

Evensen, G, Sequential data assimilation with a nonlinear quasi-geostrophic model using Monte Carlo methods to forecast error statistics, *J. Geophys. Res.*, **99**, 10143-10162, 1994.

Farrell, B.F. and P.J. Ioannou, Accurate Low-Dimensional Approximation of the Linear Dynamics of Fluid Flow, *Journal of the Atmospheric Science*, **58**, pp. 2771-2789, 2001.

Houtekammer, P.L. and H.L. Mitchell, 1998: Data Assimilation using an ensemble Kalman filter technique, **Mon. Wea. Rev.**, **126**, 796-811.

Lin, S.-J., and R.B. Rood, 1996, Multidimensional Flux-form semi-lagrangian Transport Schemes, *Mon. Wea. Rev.*, **124**, 2046-2070.

Mallat, S.G., A theory for multiresolution signal decomposition: the wavelet representation, *IEEE Transaction on Pattern Analysis and Machine Intelligence*, **11**, 675-693, 1989.

Ménard, R., Cohn, S.E., Chang, L.-P. and Lyster P.M., Stratospheric Assimilation of Chemical Tracer Observations Using a Kalman Filter, Part I: Formulation. *Mon. Wea. Rev.*, **128**, 2654-2671, 2000.

Ménard, R. and Chang, L.-P., Stratospheric Assimilation of Chemical Tracer Observations Using a Kalman Filter. Part II; χ^2 - Validated Results and Analysis of Variance and Correlation Dynamics. *Mon. Wea. Rev.*, **128**, 2672-2686.

Riishøjgaard, L.P., A direct way of specifying flow-dependent background error correlations for meteorological analysis systems, *Tellus A*, **50A**, 42-57, 1998.

Tangborn, A. and S.Q. Zhang, Wavelet Transform Adapted to an Approximate Kalman Filter System. *Appl. Num. Math.*, **33**, 307-316, 2000.

8 Figure Captions

Figure 1 - Error Covariance for the entire two-dimensional domain

Figure 2 - Schematic representation of how the error covariance for a single point (below) becomes a single column of the whole error covariance matrix (above).

Figure 3 - Assimilation results with forecast error covariance updated in wavelet space and analysis error covariance calculated in physical space. Panel (a) shows the error correlation after 8 days for the full system while panel (b) shows the correlation after 8 days with a truncation of 1024×1024 wavelet coeffficients. Panel (c) shows the mean quadratic difference in the analysis constituent fields for the truncated and full systems. The x-axis is number of 3-hour analysis cycles. The total time is about eight days.

Figure 4 - Error covariance for a point (29,13). (a) Full Covariance propagated (b) 1024×1024 truncation (c) 512×512 truncation (d) 256×256 truncation. Forecast and Analysis covariances are calculated in wavelet space for panels b-d.

Figure 5 - (a) Constituent field for the benchmark after 24 days of assimilation (in ppv). (b) Difference in mixing ratio between benchmark and 1024×1024 truncation case (c) Difference in mixing ratio field between benchmark and 512×512 truncation case (d) Difference in mixing ratio field between benchmark and 256×256 truncation case.

Figure 6 - Mean absolute error for the constituent field relative to the benchmark (full covariance evolution) for a 24 day assimilation. The error is defined as $\epsilon = \frac{1}{A} \sum_{i,j} \frac{|\mu(i,j) - \mu_{ref}(i,j)|}{\mu_{ref}(i,j)} dA_{i,j}$. Both the forecast and analysis covariances are calculated in wavelet space.

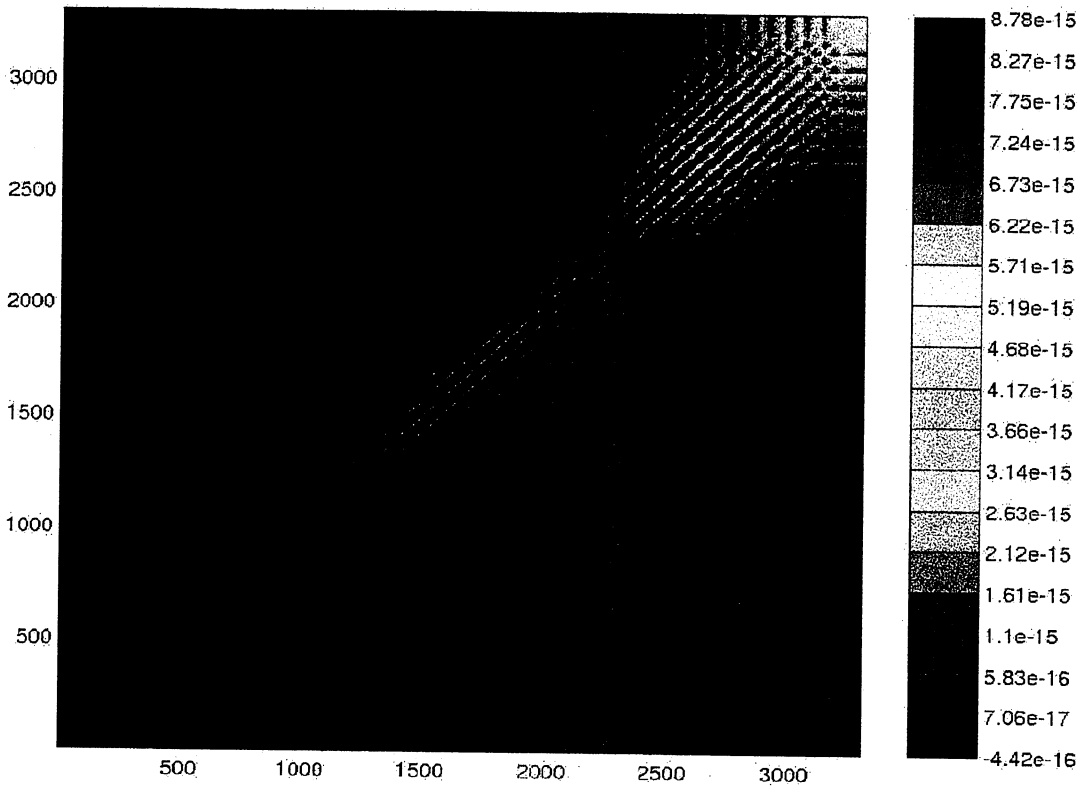

Figure 1: Error Covariance for the entire two-dimensional domain

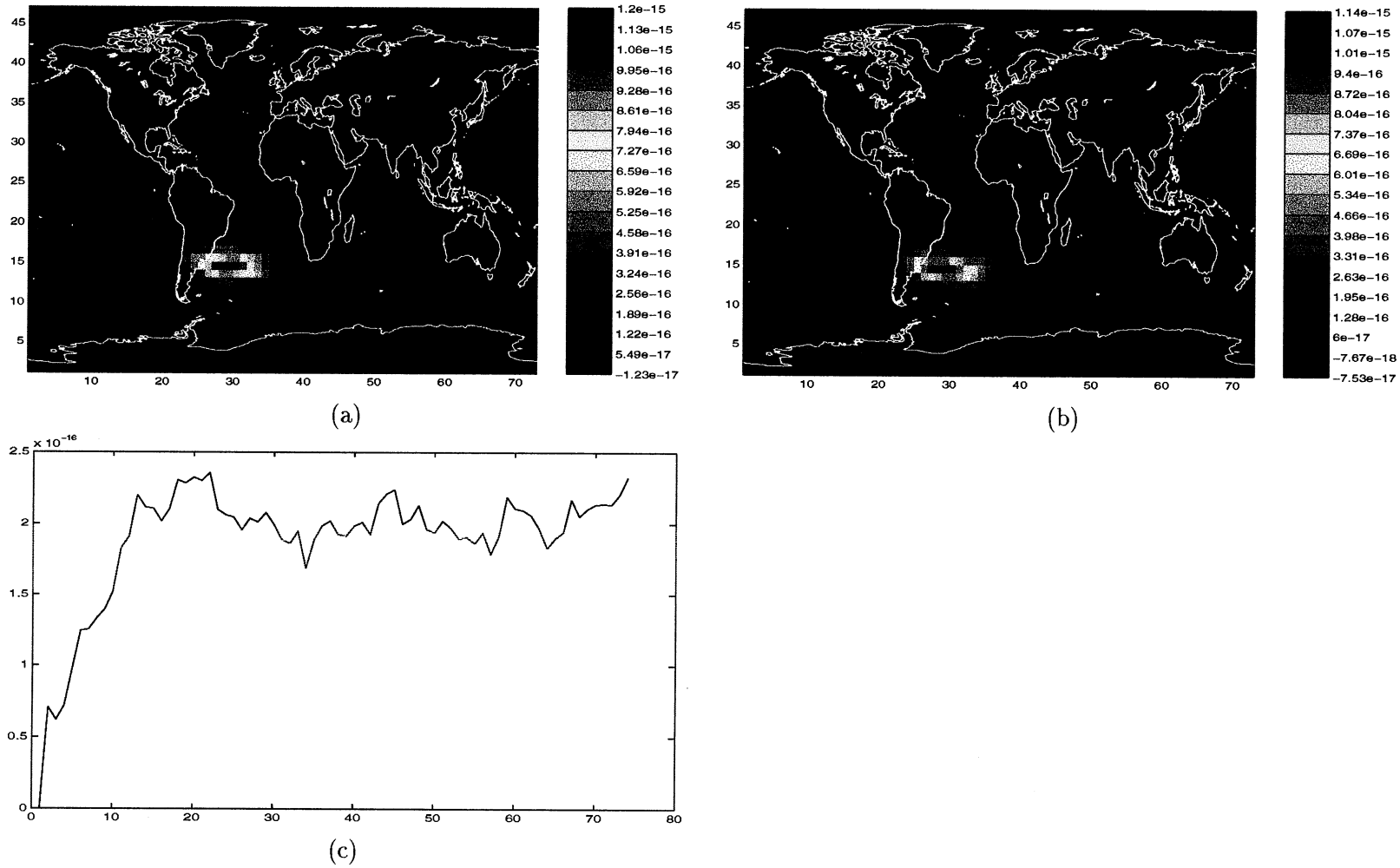

Figure 3: Assimilation results with forecast error covariance updated in wavelet space and analysis error covariance calculated in physical space. Panel (a) shows the error correlation after 8 days for the full system while panel (b) shows the correlation after 8 days with a truncation of 1024×1024 wavelet coeffficients. Panel (c) shows the mean quadratic difference in the analysis constituent fields for the truncated and full systems. The x-axis is number of 3-hour analysis cycles. The total time is about eight days.

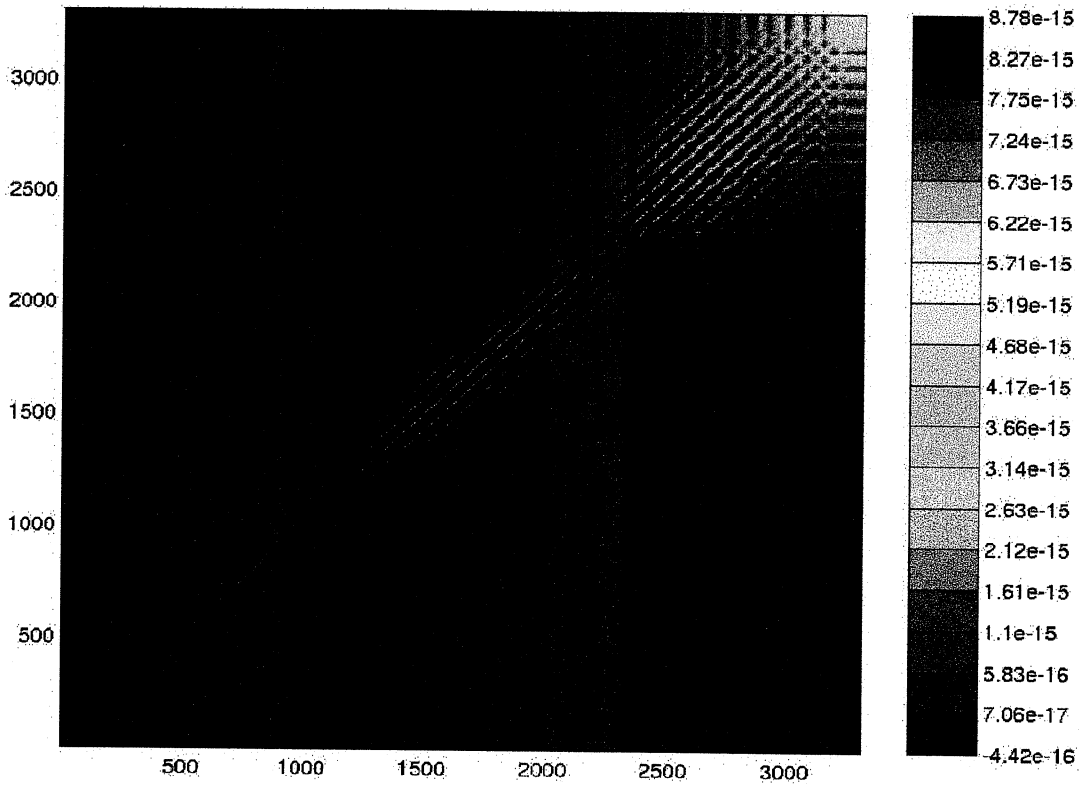

Figure 1: Error Covariance for the entire two-dimensional domain

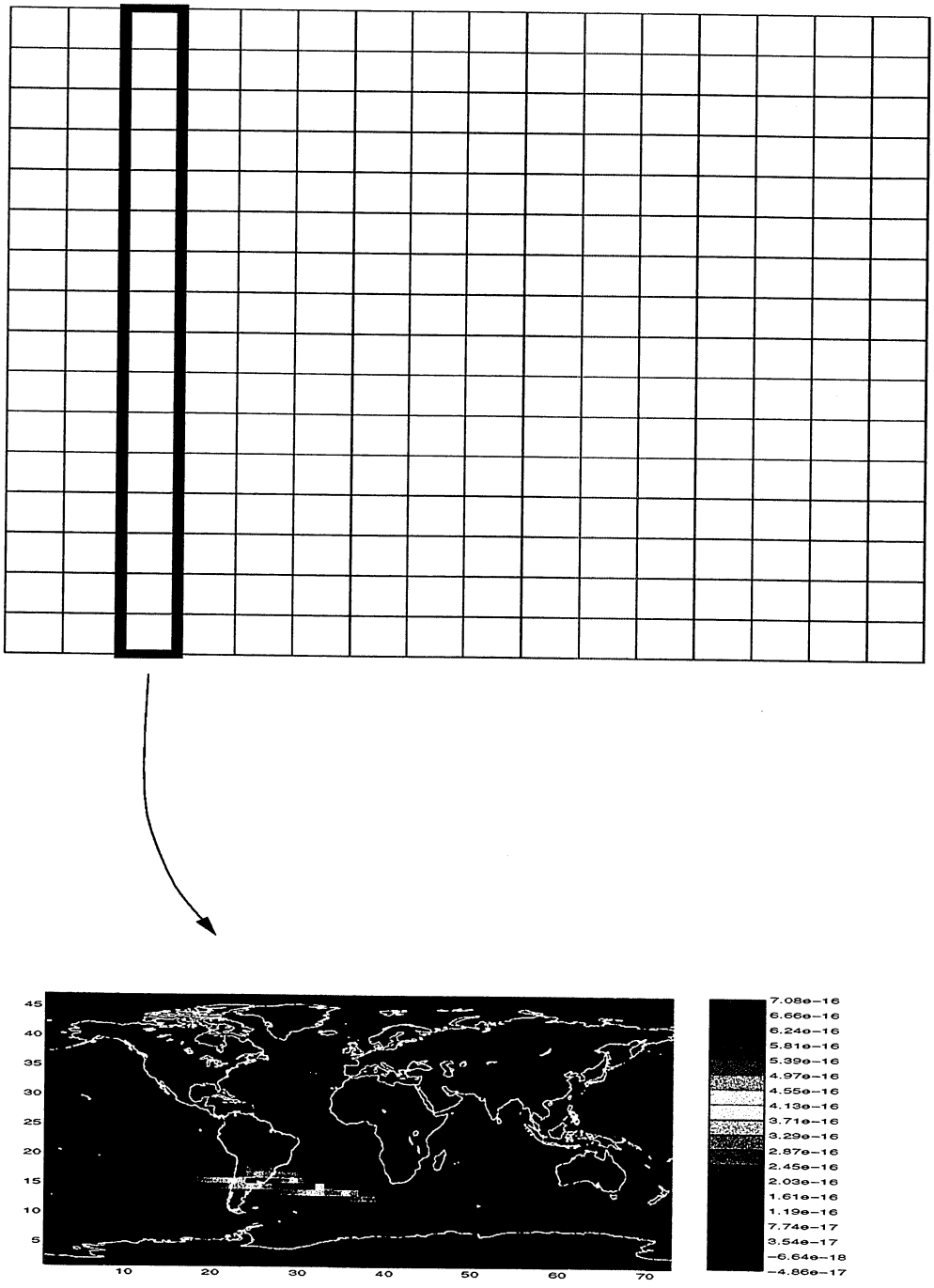

Figure 2: Schematic representation of how the error covariance for a single point (below) becomes a single column of the whole error covariance matrix (above).

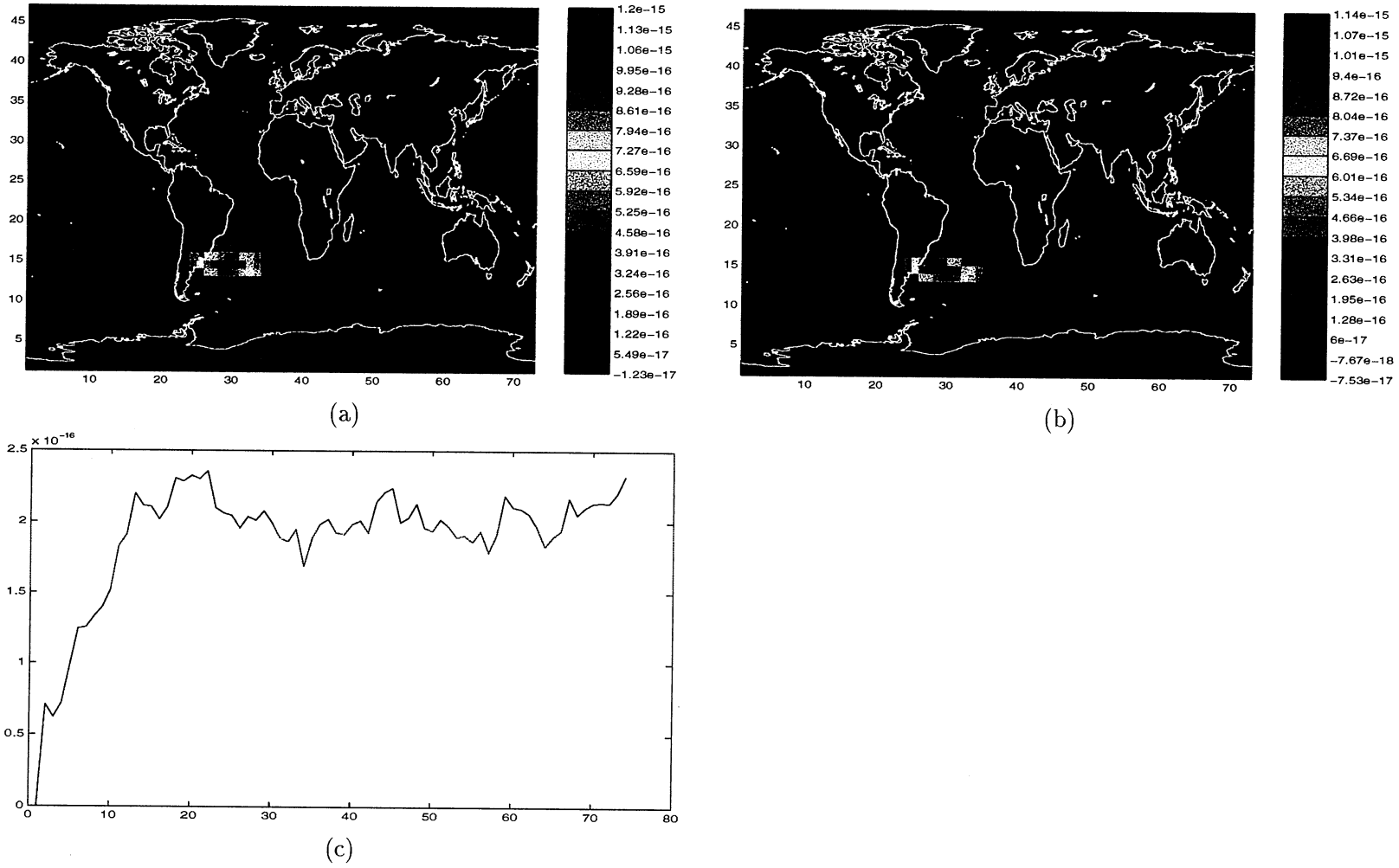

Figure 3: Assimilation results with forecast error covariance updated in wavelet space and analysis error covariance calculated in physical space. Panel (a) shows the error correlation after 8 days for the full system while panel (b) shows the correlation after 8 days with a truncation of 1024×1024 wavelet coeffficients. Panel (c) shows the mean quadratic difference in the analysis constituent fields for the truncated and full systems. The x-axis is number of 3-hour analysis cycles. The total time is about eight days.

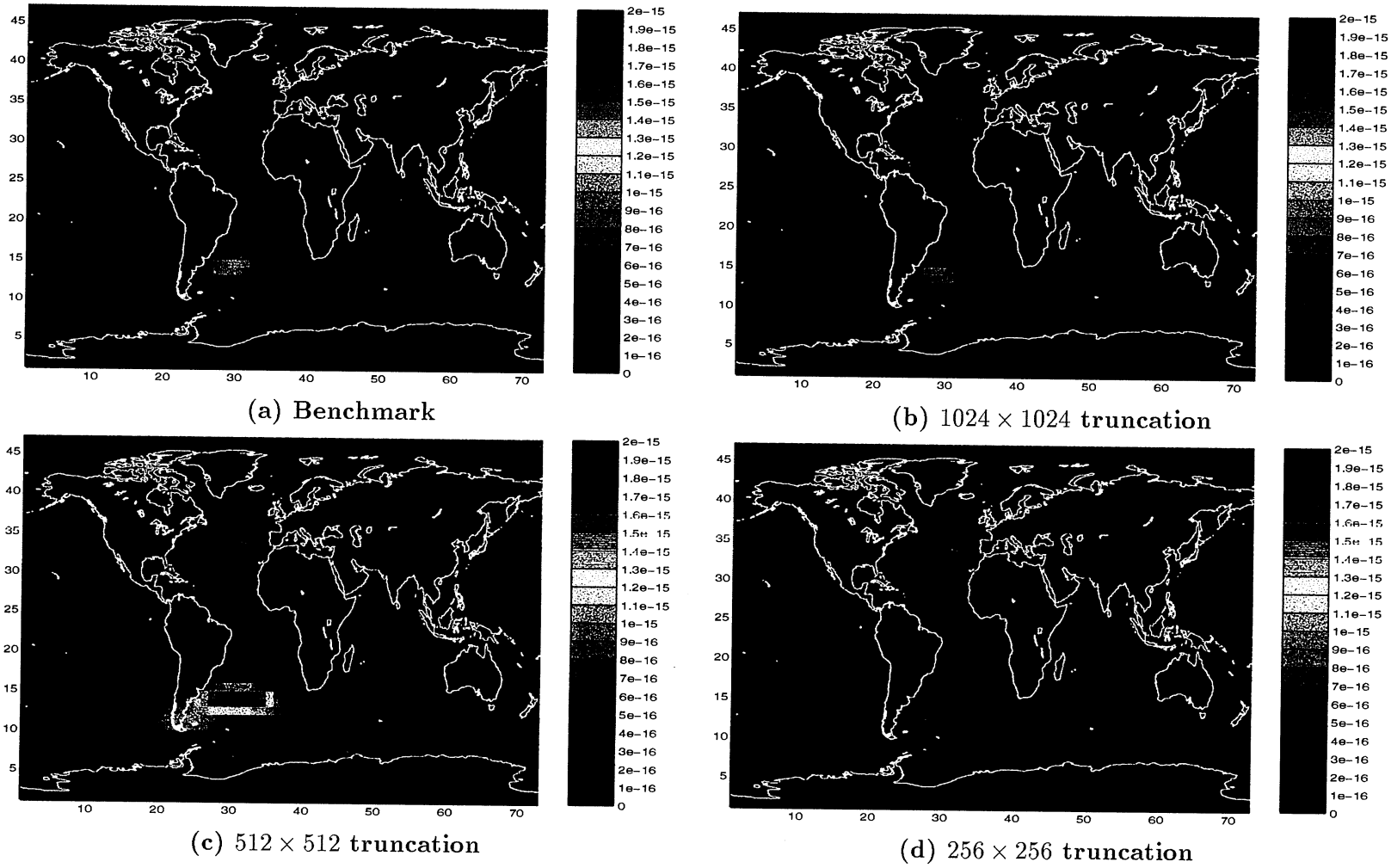

Figure 4: Error covariance for a point (29,13). (a) Full Covariance propagated (b) 1024×1024 truncation (c) 512×512 truncation (d) 256×256 truncation. Forecast and Analysis covariances are calculated in wavelet space for panels b-d.

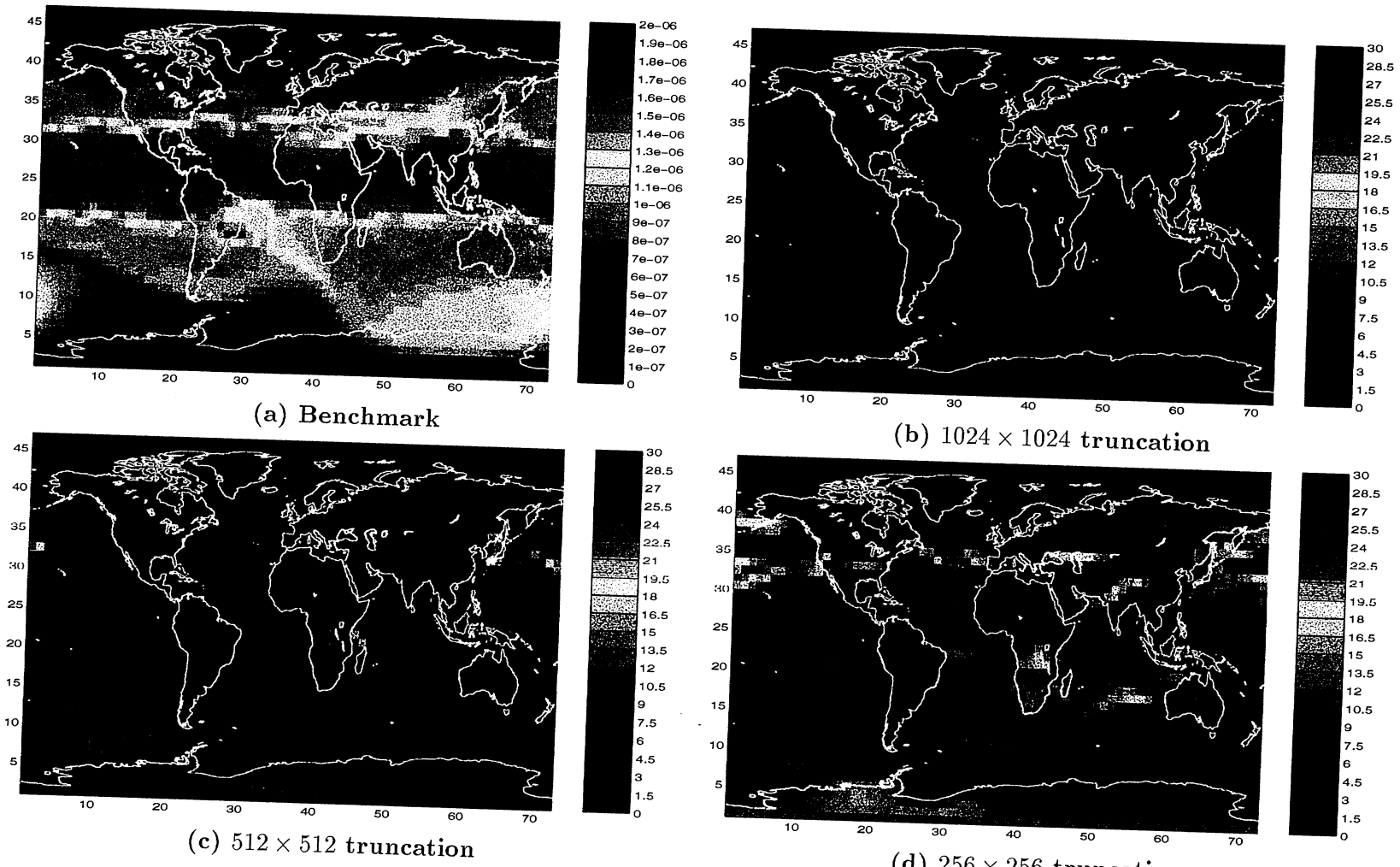

Figure 5: (a) Constituent field for the benchmark after 24 days of assimilation (in ppv). (b) Difference in mixing ratio between benchmark and 1024×1024 truncation case (c) Difference in mixing ratio field between benchmark and 512×512 truncation case (d) Difference in mixing ratio field between benchmark and 256×256 truncation case.

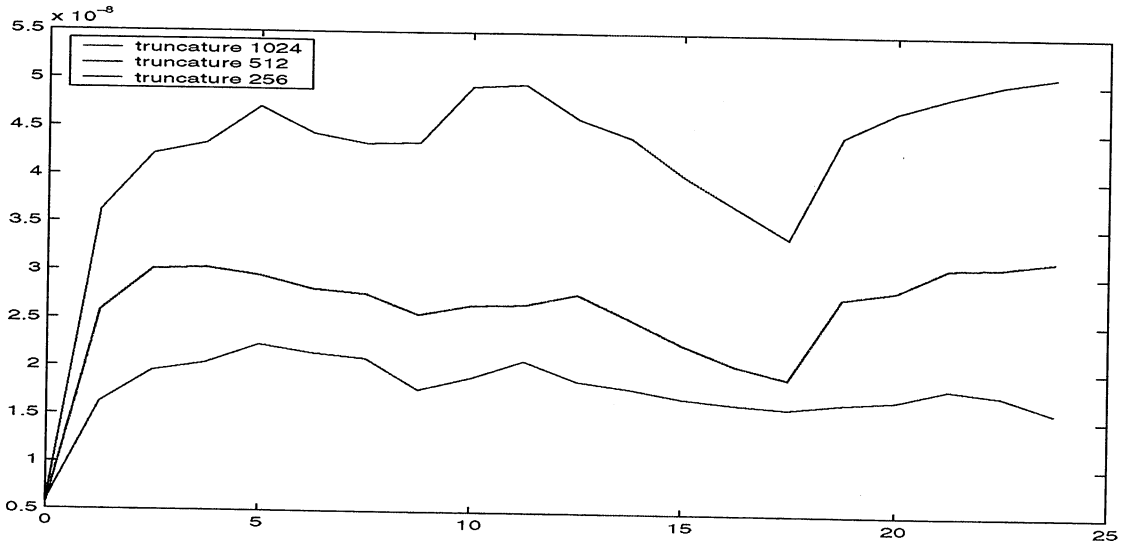

Figure 6: Mean absolute error for the constituent field relative to the benchmark (full covariance evolution) for a 24 day assimilation. The error is defined as $\epsilon = \frac{1}{A}\sum_{i,j}\frac{|\mu(i,j)-\mu_{ref}(i,j)|}{\mu_{ref}(i,j)}dA_{i,j}$. Both the forecast and analysis covariances are calculated in wavelet space.

A Wavelet Based Suboptimal Kalman Filter for Assimilation of Stratospheric Chemical Tracer Observations

Ludovic Auger
and
Andrew Tangborn

The Kalman filter is a method which combines information from atmospheric measurements and numerical weather forecasts in an optimal way, so that the maximum information is extracted from the two sources and the best estimate of the state of the atmosphere is obtained. This optimal estimate is dependent on both accurate knowledge of error statistics (model and observation) and the means to evolve these statistics in time, in the form of an error covariance. Both of these requirements are major hurdles that have kept the Kalman filter from general use in large scale data assimilation systems. In this work we focus on a technique to overcome the latter difficulty, which is one of excessive computational expense.

In this work we demonstrate a technique for approximating both the error covariance and the discretized dynamical equations for evolving them using the discrete wavelet transform. Wavelets are orthogonal sets of functions that are local in location and scale. We show that many of the important structures in these matrices can be represented by a relatively small number of wavelet coefficients, thus allowing substantial compression of the system of equations.

This technique is demonstrated on a system that assimilates chemical species observations from CLAES and HALOE into a two-dimensional global transport model. We show that nearly optimal assimilation can be obtained with the covariance evolution equations reduced in size by about 90 % and the computational cost of the entire Kalman filter is reduced by 80 %.